Flipping the GPCR Switch: Structure–Based Development of Selective Cannabinoid Receptor 2 Inverse Agonists

Miroslav Kosar,[a] Roman C. Sarott,[a] David A. Sykes,[b] Alexander E. G. Viray,[c] Rosa Maria Vitale,[d] Nataša Tomašević,[e] Xiaoting Li,[f] Rudolf L. Z. Ganzoni,[a] Bilal Kicin,[a] Lisa Reichert,[a] Kacper J. Patej,[a] Uxía Gómez-Bouzó,[a] Wolfgang Guba,[g] Peter J. McCormick,[h] Tian Hua,[f] Christian W. Gruber,[e] Dmitry B. Veprintsev,[b] James A. Frank,*[c,i] Uwe Grether,*[g] and Erick M. Carreira*[a]

[a]Laboratorium für Organische Chemie, Eidgenössische Technische Hochschule Zürich, Vladimir-Prelog-Weg 3, 8093 Zürich, Switzerland
[b]Faculty of Medicine & Health Sciences, University of Nottingham, Nottingham NG7 2UH, UK; Centre of Membrane Proteins and Receptors (COMPARE), University of Birmingham and University of Nottingham, Midlands, UK
[c]Department of Chemical Physiology & Biochemistry, Oregon Health & Science University, Portland, Oregon 97239-3098, United States
[d]Institute of Biomolecular Chemistry, National Research Council, Via Campi Flegrei 34, 80078 Pozzuoli, Italy
[e]Center for Physiology and Pharmacology, Medical University of Vienna, Schwarzspanierstr. 17, 1090 Vienna, Austria
[f]iHuman Institute, ShanghaiTech University, Shanghai 201210, China.
[g]Roche Pharma Research & Early Development, Roche Innovation Center Basel, F. Hoffmann-La Roche Ltd., 4070 Basel, Switzerland
[h]Centre for Endocrinology, William Harvey Research Institute, Queen Mary University of London, London, UK
[i]Vollum Institute, Oregon Health & Science University, Portland, Oregon 97239-3098, United States

ABSTRACT

We report the structure-based design of cannabinoid receptor type 2 (CB_2R)-selective inverse agonists (*S*)-**1** and (*R*)-**1**, which were derived from privileged agonist HU-308 by introduction of a phenyl group at the *gem*-dimethylheptyl sidechain. Epimer (*R*)-**1** exhibits high affinity for CB_2R with K_d = 39 nM and serves as a platform for the synthesis of a wide variety of probes. Notably, the fluorescent probes, for the first time, retain their inverse agonist functionality, high affinity, and selectivity for CB_2R independent of linker and fluorophore substitution. Ligands (*S*)-**1**, (*R*)-**1**, and their derivatives act as inverse agonists in CB_2R-mediated cAMP as well as G protein recruitment assays, and do not trigger β-arrestin–receptor association. Furthermore, no receptor activation was detected in live cell $ERK_{1/2}$ phosphorylation and Ca^{2+}-release assays. Confocal fluorescence imaging experiments with (*R*)-**7 (**Alexa488) and (*R*)-**9** (Alexa647) probes employing BV-2 microglial cells visualized CB_2R expressed at endogenous levels. Finally, molecular dynamics simulations corroborate the initial docking data in which inverse agonists restrict movement of toggle switch, $Trp258^{6.48}$, and thereby stabilize CB_2R in its inactive state. The present study

serves as a blueprint for the rational design of GPCR ligands beyond CB_2R with a tailored functional response.

INTRODUCTION

The endocannabinoid system is present in all vertebrates and comprises endogenous ligands, enzymes mediating ligand metabolism, transporters and two prominent cannabinoid receptors type 1 and 2 (CB_1R and CB_2R).[1] Exploitation of the therapeutic potential of CB_2R has primarily focused on receptor activation with agonists and showed promise to ameliorate a plethora of diseases, such as autoimmune[2] and metabolic disorders,[3] chronic pain,[4] multiple sclerosis,[5] and cancer.[6] By contrast, CB_2R antagonists and inverse agonists remain vastly underexplored entities despite encouraging results in models of renal fibrosis,[7] arthritis,[8] and neuroinflammation.[9]

Although there is a current renaissance of clinical trials pursuing development of selective CB_2R therapeutics,[10] to date there are no such drugs available on the market. This absence stems from poor understanding of CB_2R localization, expression, and signaling on the molecular level.[11] Elucidation of CB_2R pharmacology has been hampered by insufficient specificity of monoclonal antibodies[12] and scarcity of reliable chemical probes.[13] Although some potent, selective, and validated fluorescent probes have been reported,[14] these function as agonists that disturb cellular homeostasis by triggering downstream signaling and β-arrestin association, followed by agonist-mediated receptor internalization.[15] These limitations may be addressed by implementation of inverse agonist-based fluoroprobes that do not prompt receptor endocytosis. Additionally, inverse agonists engage with receptors in the more populous inactive GPCR conformation, leading to improved signal-to-noise ratio in comparison to agonists.[16]

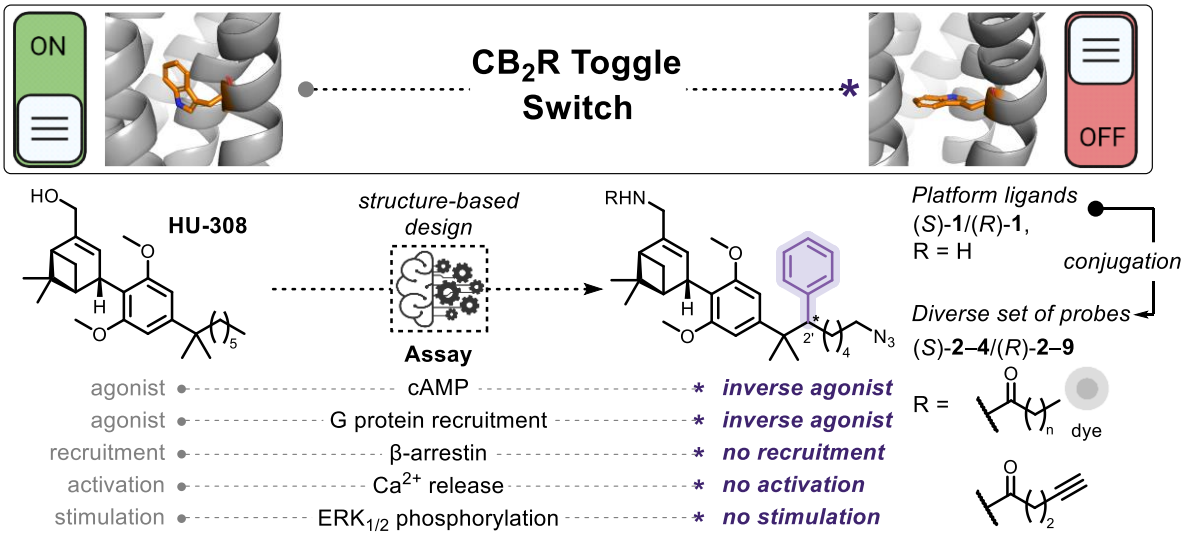

Scheme 1. Herein reported novel structure-based design of HU-308-derived CB_2R-selective inverse agonists.

Historically, development of high-affinity, selective fluorescent CB_2R inverse agonists has proven arduous. In the cases reported, fluorophore conjugation completely ablated[17] or materially reduced[18] affinity. In one example, a study of a series of agonists led to the identification of a specific linker-fluorophore construct endowing inverse agonism.[19] Development of a potent, selective, and versatile CB_2R-targeting inverse agonist scaffold that could be conjugated to a variety of fluorophores and functionalities remains an unmet challenge.

Since its discovery in 1999,[20] CB_2R-selective agonist HU-308 (Scheme 1) has enjoyed privileged status for the study of CB_2R pharmacology.[21] HU-308 has been extensively applied to unravel effects of CB_2R activation in animal models of pain,[22] osteoporosis,[23] Parkinson's disease,[24] amyotrophic lateral sclerosis,[25] and is currently investigated in Phase I clinical trials for mitigation of inflammation.[26] The pharmacophore embedded in HU-308 has served in the development of photoswitchable,[27] fluorescent,[14c,28] and ligand-directed covalent probes.[14a] On the basis of our prior work with HU-308, we focused on this scaffold with the intent of transforming its functional profile from agonist to inverse agonist with minimal structural modification. Notably, Schapira and Jones have independently discussed the benefits of working with a set of molecules closely related in structure to enable in depth understanding of receptor pharmacology.[29]

The past two decades witnessed an exponential rise of published GPCR structures, hence structure-based ligand design is at present ideally positioned to capitalize on the ongoing revolution.[30] GPCRs of the most populous class A family are distinguished by high homology of the CWxP motif. In particular, the toggle switch of CWxP that modulates receptor activation, Trp258$^{6.48}$, is

conserved within 78% of non-olfactory GPCRs.[31] Since more than a third of all approved drugs exert their action by GPCR modulation, it is vital to comprehensively investigate and understand receptors' pharmacology with functionally orthogonal chemical probes.[32] Examination of the X-ray structure of CB_2R in its inactive conformation revealed a secondary binding pocket that hosts $Trp258^{6.48}$. In silico docking studies suggested that addition of a substituent at C(2') of HU-308 might constrain $Trp258^{6.48}$ and hence modulate CB_2R activation (Scheme 1).

The novel inverse agonists described herein emerged as avid binders of CB_2R with excellent selectivity over the closely related CB_1R. The compounds were profiled for their functional response in a comprehensive panel of in vitro (cAMP, β-arrestin and G protein recruitment) as well as cellular ($ERK_{1/2}$ phosphorylation, Ca^{2+} signaling) assays. Remarkably, none of the probes activate CB_2R in any of the tested pathways. Fluorescent probes demonstrated excellent specificity and visualized CB_2R expressed at endogenous levels in live-cell confocal microscopy experiments. Finally, molecular dynamics simulations investigated structural determinants that prevent receptor activation upon ligand binding and corroborate movement restriction of $Trp258^{6.48}$. The workflow and key considerations described herein may be used to successfully drive future structure-based switch of functionality involving ligands and proteins beyond HU-308 and CB_2R.

RESULTS AND DISCUSSION

In Silico Probe Design

We have investigated the recently published active (PDB:8GUS, Figure 1A)[33] and inactive (PDB:5ZTY, Figure 1B)[34] conformations of CB_2R crystallized with agonist HU-308 and the antagonist/inverse agonist AM10257, respectively. Close examination of the two receptor conformations revealed that AM10257 reaches into a secondary binding pocket that features a highly conserved CWxP motif in class A GPCRs,[35] and moreover hosts $Trp258^{6.48}$, the recently designated single residue toggle switch of CB_2R activation.[36]

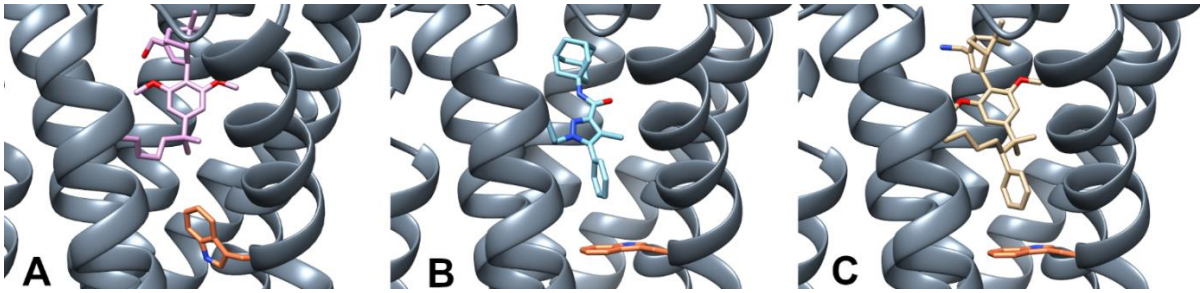

Figure 1. Comparison of the active (**A**, PDB: 8GUS, ligand: HU-308)[33] and inactive (**B**, PDB: 5ZTY, ligand: AM10257)[34] CB_2R conformations. (**C**) Docking study of HU-308-derived putative inverse agonist (*R*)-**1** in the inactive CB_2R conformation (PDB: 5ZTY). (*R*)-**1** reaches into the secondary pocket occupied by the toggle switch responsible for CB_2R activation, $Trp258^{6.48}$ (orange), and shares virtually identical binding mode as AM10257.

Comparison of the two receptor conformations combined with in silico docking suggested that a phenyl substituent introduced α to the *gem*-dimethyl group of HU-308 might occupy the same lipophilic sub-pocket as AM10257. The phenyl motif creates a new C(2') stereocenter at the pendant side chain; henceforth the explicit (*S*)- and (*R*)- designations preceding compound labels denote its absolute configuration. We have additionally incorporated structural features, which proved critical in our prior works to bestow an excellent pharmacological profile, yielding ligands (*S*)-**1** and (*R*)-**1** (Scheme 2).[14a,c,28] Namely, we have substituted the allylic alcohol for an amine and inserted a terminal azide to allow facile, stable conjugation to fluorophores and confer improved affinity and selectivity for CB_2R. The novel putative HU-308-derived inverse agonist (*R*)-**1** showed virtually identical binding interactions as AM10257 in the inactive CB_2R conformation (Figure 1C). In particular, the C(2') phenyl group of (*R*)-**1** oriented toward $Trp258^{6.48}$ and attained a similar favorable edge-to-face π-interaction as the phenyl of AM10257. The nearly identical interactions are essential as we hypothesized that the impediment of the upward movement of $Trp258^{6.48}$ could effectively prevent receptor activation.

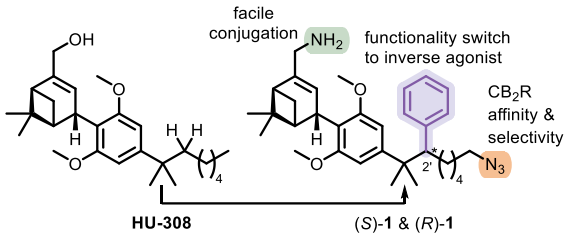

Scheme 2. Design of inverse agonists (*S*)-**1** and (*R*)-**1**.

Synthesis

Access to (*S*)-**1** and (*R*)-**1** that feature a phenyl group at the homobenzylic position α to a sterically demanding *gem*-dimethyl group is synthetically challenging and unprecedented. Prior structure–activity relationship studies on cannabinoid ligands focused almost exclusively on the easily accessible benzylic or ω-position of the pendant side chain.[37] To the best of our knowledge, there is only a single report of substitution at the homobenzylic position with a methyl group in a structure of Δ^8-THC that lacks the sterically congesting *gem*-dimethyl motif.[38]

The synthesis of (*S*)-**1**/(*R*)-**1** commenced with **10**, which was accessed by methylation of 3,5-dimethoxyphenylacetonitrile and subsequent treatment with phenyl lithium (Scheme 3).[39] Introduction of the alkyl side chain to ketone **10** proved a formidable challenge due to the steric hindrance. Initial attempts using established phosphonium ylide routes yielded no reaction even at elevated temperatures.[40] An extensive screening of Grignard reagents either yielded no reaction or afforded exclusively the Grignard reduction product **11**. Finally, using a modified procedure for the preparation of alkyl lithiums by Punzalan,[41] we employed, for the first time, 5-chloropentyl lithium to forge the tertiary alcohol **12** in 83% yield. Subsequent Chugaev elimination of the benzylic alcohol under mild conditions yielded **13** as a single *E*-diastereomer in 95% yield. BBr_3-mediated demethylation followed by high-pressure hydrogenation over Pd/C afforded (*S*)-**14**/(*R*)-**14** as a racemic mixture in 94% yield over two steps. The synthesis was continued with the racemate to rapidly access material for initial pharmacological evaluation. To this end, Friedel-Crafts allylation with verbenol derivative **15** followed by treatment with $(MeO)_2SO_2$ furnished methylated epimeric mixture (*S*)-**16**/(*R*)-**16** in 50% yield over the two steps. Subsequent substitution of the primary alkyl chloride with NaN_3 and hydrazine mediated phthalimide deprotection revealed allylic amines (*S*)-**1**/(*R*)-**1** in 73% yield. Finally, the synthesis concluded by functionalization of the diastereomeric mixture (*S*)-**1**/(*R*)-**1** with DY-480XL or 4-pentynoic acid to yield mixtures of epimers (*S*)-**2**/(*R*)-**2** and (*S*)-**3**/(*R*)-**3**, respectively.

We then investigated access to epimers (*S*)-**1** and (*R*)-**1** separately. Following introduction of the verbenol fragment **15**, comprehensive screening of conditions to separate the resulting epimers ((*S*)-**16**/(*R*)-**16**) by silica gel chromatography, HPLC, and SFC proved unsuccessful. Gratifyingly, we found that enantiomers (*S*)-**14**/(*R*)-**14** could be separated by semi-preparative supercritical fluid chromatography (SFC) using a chiral stationary phase to yield (*S*)-**14** and (*R*)-**14** in >99% *ee* and 96% *ee*, respectively. Resorcinols (*S*)-**14** and (*R*)-**14** were then functionalized to yield enantio- and diastereomerically pure (*S*)-**1**–**4** and (*R*)-**1**–**9**. To assign the absolute configuration at the C(2') stereocenter (*S*)-**14** was converted to a *p*-nitrobenzoate (*S*)-**17**, whose structure was elucidated by X-ray crystallography.

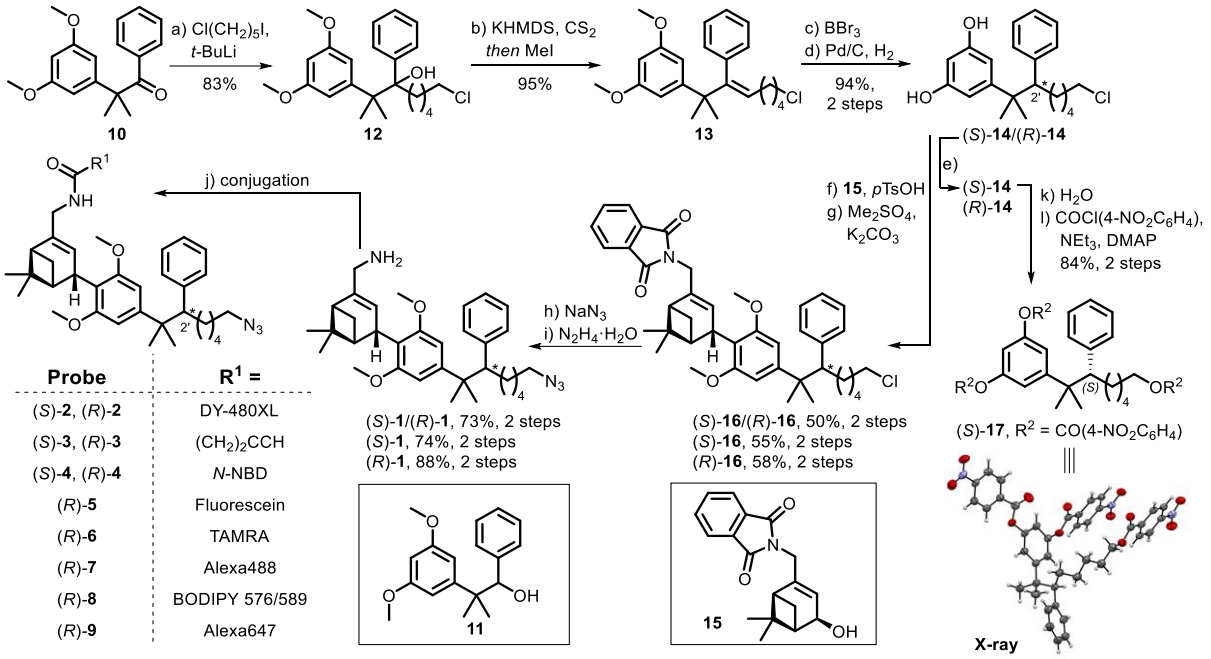

Scheme 3. Synthesis of novel CB_2R-selective HU-308-derived inverse agonists.[a]

[a]Reagents and conditions: (a) 1-chloro-5-iodopentane, *t*-BuLi, *n*-pentane, Et_2O, –78 °C to rt, 83%; (b) KHMDS, CS_2, THF, –78°C to rt *then* MeI, 40°C, 95%; (c) BBr_3, CH_2Cl_2, 0 °C, 97%; (d) Pd/C, H_2, EtOAc, rt, 97%; (e) semi-preparative SFC, (*S*)-**14**, 25%, >99% *ee*, (*R*)-**14**, 20%, 96% *ee*; (f) **15**, *p*TsOH·H_2O, CH_2Cl_2, rt, 64%–71%; (g) $(MeO)_2SO_2$,K_2CO_3, acetone, rt, 78%–82%; (h) NaN_3, DMF, 50 °C, 88%–96%; (i) N_2H_4·H_2O, (*E*)/(*Z*)-crotyl alcohol, EtOH, 75 °C, 76%–94%; (j) conjugation; (k) H_2O, microwave irradiation, 150 °C, 99%; (l) 4-nitrobenzoyl chloride, NEt_3, DMAP, CH_2Cl_2, rt, 85%

In Vitro Pharmacological Profiling

Saturation Binding Assays

We assessed whether the phenyl substitution in (*S*)-**1**, (*R*)-**1** and their derivatives (*S*)-**2–4**, (*R*)-**2–9** impedes interaction with CB_2R. To this end, time-resolved Förster resonance energy transfer (TR-FRET) binding assay was employed to determine affinity of the new probes at room temperature.[14c] HEK293 membrane preparations of SNAP-Lumi4-Tb labelled hCB_2R were incubated with a fluorescent probe in presence or absence of a validated inverse agonist, SR-144,528,[21] to determine its binding parameters. Gratifyingly, the epimeric mixture (*S*)-**2**/(*R*)-**2** demonstrated good affinity for CB_2R (K_d = 67.9 nM), thus implying the C(2') functionalization was well tolerated and validated the in silico-guided design.

Encouraged by the promising result, we studied the impact of configuration at the C(2') stereocenter on the pharmacological properties by examining each epimer individually. A 12-fold greater binding affinity for CB_2R was shown by (*R*)-**1** (K_d = 39.1 nM) in comparison to (*S*)-**1** (K_d = 476 nM). Functionalization of (*S*)-**1** and (*R*)-**1** with 4-pentynoic acid retained the stereoisomeric preference and

yielded exceptionally avid CB_2R binders (*S*)-**3** and (*R*)-**3**, K_d = 2.10 nM and 0.42 nM, respectively. Conjugation of (*S*)-**1** and (*R*)-**1** with DY-480XL and *N*-NBD yielded probes (*S*)-**2**, (*R*)-**2** and (*S*)-**4**, (*R*)-**4**, respectively. Fluoroprobes (*S*)-**2** and (*S*)-**4** displayed inferior CB_2R affinity (CB_2R K_d = 162 nM and 158 nM, respectively) compared to the excellent binding potency of (*R*)-**2** and (*R*)-**4** (CB_2R K_d = 10.2 nM and 12.3 nM, respectively). Furthermore, strong agreement was observed between K_d and K_i values obtained by independent TR-FRET and radioligand binding assays for (*R*)-**2** (CB_2R K_d = 10.2 nM and K_i = 8.26 nM, respectively) and (*R*)-**3** (CB_2R K_d = 0.42 nM and K_i = 0.66 nM, respectively). Collectively, the results further validate the TR-FRET assay and imply that the orthosteric binding pocket of CB_2R shows preference for the *R*-epimer of the parent compound and its derivatives.

We then set out to investigate whether the excellent CB_2R affinity of (*R*)-**1–4** is impacted by linker and fluorophore substitution. To this end, probes (*R*)-**5–9** were prepared that feature a variety of linker lengths and fluorophores, spanning a wide range of size, lipophilicity, and membrane permeability. When tested by TR-FRET at 37 °C, fluorescein, tetramethylrhodamine (TAMRA), and Alexa488 bearing probes (*R*)-**5**, (*R*)-**6**, and (*R*)-**7** all emerged as high affinity binders for CB_2R with excellent K_d values of 30.3 nM, 2.78 nM, and 24.9 nM, respectively (Table 1). BODIPY 576/589 conjugate (*R*)-**8** showed good binding potency with CB_2R K_d = 44.7 nM. Particularly remarkable was the excellent affinity of probe (*R*)-**9** (K_d = 25.9 nM) functionalized with Alexa647. These results illustrate substantial improvement over previous work where functionalization with the highly polar Alexa488 and sterically demanding Alexa647 led to 64–fold and 611–fold drop in affinity, respectively.[14c] Importantly, fluoroprobes (*R*)-**5**, (*R*)-**6**, (*R*)-**7**, and (*R*)-**9** emit robust fluorescence signals with exquisite specific binding windows when tested at physiologically relevant temperature, 37 °C (see Figure 2 and SI Figure S1).

Table 1. TR-FRET-Based Profiling of Binding Affinity‡

Probe	Dye	K_d [nM]‡		
		CB_2R	CB_1R	K_d ratio (CB_1R/CB_2R)
(*R*)-**2**	DY-480XL	18.9	1740	92
(*R*)-**5**	Fluorescein	30.3	1280	42
(*R*)-**6**	TAMRA	2.78	396	142
(*R*)-**7**	Alexa488	24.9	3300	133
(*R*)-**9**	Alexa647	25.9	7050	272

‡Saturation binding data (K_d) were determined in a TR-FRET assay at 37 °C with membrane preparations from either hCB_2R-HEK293 or hCB_1R-HEK293 cells. $N = 3$.

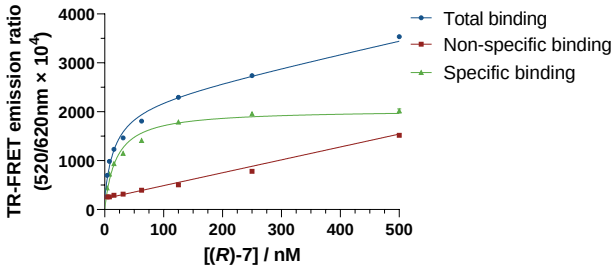

Figure 2. TR-FRET-based saturation binding profile of (*R*)-**7** (Alexa488) at CB_2R determined at 37°C. Non-specific binding was determined in presence of SR-144,528 (10 μM). Mean ± SEM, $N = 3$

Binding selectivity of fluorescent probes was tested against the closely related CB_1R in a saturation binding assay at 37 °C using membrane preparations derived from HEK293 cells expressing hCB_1R (Table 1). Fluoroprobes (*R*)-**2**, (*R*)-**5**, (*R*)-**6**, and (*R*)-**7** displayed 92-fold, 42-fold, 142-fold, and 133-fold selectivity for CB_2R over CB_1R, respectively. Notably, (*R*)-**9** demonstrated an exceptional 272-fold preference for CB_2R over CB_1R. Collectively, the excellent affinity and selectivity of a range of physicochemically distinct substituents and fluorophores highlight the versatility of novel platform ligand (*R*)-**1**.

Kinetic Binding TR-FRET Assay

We were intrigued by the performance of our probes in the saturation binding assay and leveraged TR-FRET to study ligand binding kinetics at physiologically relevant temperature, 37 °C (Table 2). The results suggest that all compounds, except (*S*)-**1**, possess dramatically slower receptor dissociation rates, k_{off}, in comparison to control inverse agonist SR-144,528. Therefore, high CB_2R affinity of the probes stems from slow receptor dissociation rates once bound. The probes are thus endowed with long receptor residence times, τ, an attribute that has been argued particularly important for GPCRs[42] as a better suited determinant, compared to K_d, of ligand-protein interactions in living systems.[43] Importantly, excellent agreement was found between K_d values obtained in saturation and kinetic binding experiments.

Table 2. TR-FRET-Based Kinetic Profiling of Probes at CB_2R[‡]

Probe	k_{on} [10^6 M^{-1} min^{-1}]	k_{off} [10^{-2} min^{-1}]	τ [min]	Kinetic K_d [nM]
(*S*)-**1**	9.39	115	0.87	122
(*R*)-**1**	12.0	13.9	7.19	11.6
(*S*)-**3**	44.3	4.96	20.2	1.12
(*R*)-**3**	88.7	2.29	43.7	0.26
(*R*)-**6**	3.60	1.08	92.6	3.00
(*R*)-**7**	1.49	2.37	42.2	15.9
(*R*)-**9**	1.75	1.71	58.5	9.78
SR-144,528	240	122	0.81	5.08

[‡]Kinetic K_d data were measured at 37 °C in a TR-FRET assay using membrane preparations from hCB_2R-HEK293 cells. $N = 3$.

In Vitro Functional Profiling: cAMP, G Protein Recruitment and β-Arrestin

HU-308 is a potent full agonist at CB_2R in the [^{35}S]-GTPγS assay, triggers inhibition of cAMP production, promotes recruitment of β-arrestin, stimulates $ERK_{1/2}$ phosphorylation, and facilitates release of Ca^{2+} from intracellular stores.[21,27,44] Compounding evidence indicates that distinct CB_2R agonists favor discrete receptor conformations, leading to preferential activation of one specific signaling pathway over another, a phenomenon known as biased agonism.[21,45] Accordingly, we have dedicated substantial efforts to comprehensively profile the pharmacological response elicited by the new probes across known CB_2R signaling pathways.

One of the canonical signaling pathways of CB_2R involves association with $G\alpha_{i/o}$-proteins, which elicit reversible inhibition of adenylyl cyclase resulting in a decrease of cAMP levels and suppression of protein kinase A activity.[1a] Consequently, we have investigated the change in cAMP levels upon probe addition using homogeneous time resolved fluorescence (HTRF) cAMP assay (Table 3).

Table 3. Functional Characterization in a CB_2R cAMP Assay[‡]

Probe	pEC_{50}	E_{max}/ %
(*S*)-**1**	5.57 ± 0.45	–44.0 ± 21.3
(*R*)-**1**	6.95 ± 0.13	–44.3 ± 3.72
(*S*)-**2**	6.47 ± 0.24	–37.1 ± 6.42
(*R*)-**2**	7.15 ± 0.12	–30.7 ± 2.54
(*S*)-**3**	7.39 ± 0.14	–48.6 ± 4.61
(*R*)-**3**	7.48 ± 0.12	–55.1 ± 4.35
(*S*)-**4**[§]	4.98 ± 0.14	+44.3 ± 15.0
(*R*)-**4**	5.91 ± 0.22	–40.4 ± 7.84
ago-3	8.47 ± 0.08	+112 ± 5.03

‡Potency (pEC_{50}) and E_{max} data were obtained in a cAMP HTRF assay using hCB_2R-CHO cells. Data were normalized to agonist CP-55,940 response (100%) and basal level (0%), unless noted otherwise. §Data were normalized to the response of inverse agonist AM10257 (0%) and basal level (100%). Data shown as a mean ± SEM, $N = 3$.

All compounds behaved as inverse agonists, with efficacy (E_{max}) ranging between –30.7% to –55.1%. Both epimers of the parent amine ligand inhibited cAMP production with the (*R*)-**1** stereoisomer demonstrating greater potency (pEC_{50} = 6.95) than (*S*)-**1** (pEC_{50} = 5.57). DY-480XL and alkyne functionalized probes, (*R*)-**2** (pEC_{50} = 7.15) and (*R*)-**3** (pEC_{50} = 7.48) were favored over (*S*)-**2** (pEC_{50} = 6.47) and (*S*)-**3** (pEC_{50} = 7.39) with respect to potency, albeit to a lesser degree. Interestingly, the *N*-NBD probes (*R*)-**4** and (*S*)-**4** behaved as inverse agonists only at high concentration (pEC_{50} = 4.98 and 5.91, respectively). As a control, we prepared HU-308-derived agonist probe **ago-3** from **ago-NH$_2$** that features the same scaffold as (*S*)-**3** and (*R*)-**3** except that it lacks the C(2') phenyl substituent (Scheme 4). In the cAMP assay **ago-3** displayed potent receptor activation (pEC_{50} = 8.47, E_{max} = 112%). These results provide direct experimental evidence as to the critical role of the phenyl substituent in facilitating the switch in ligand functionality from agonist to inverse agonist.

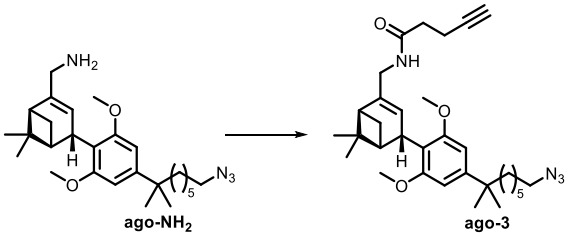

Scheme 4. Design of a control agonist **ago-3**.

To complement the functional response elicited in the cAMP assay, we tested whether the probes trigger association of $G\alpha_i$ protein with CB_2R using our recently reported bioluminescence resonance energy transfer (BRET) Gi-CASE assay.[46] Membrane preparations harvested from hCB_2R-HEK293 T-REx cells that genetically incorporate fluorescence NanoLuciferase donor and Venus acceptor proteins to the Gα and Gɣ subunits, respectively, were incubated with a probe and the change in BRET signal was detected. Agonist binding triggers CB_2R activation and dissociation of the Gα and Gβɣ subunits resulting in BRET signal reduction. Conversely, inverse agonists elicit increase in BRET intensity by stabilization of inactive CB_2R conformation and G protein accumulation beyond the basal level. Compounds (*S*)-**1**, (*R*)-**1**, (*S*)-**3**, and (*R*)-**3** were selected as representatives to circumvent interference among fluorophores in the BRET assay as previously reported.[19]

The results indicate that all tested compounds behave as potent inverse agonists with respect to G protein recruitment at CB_2R (Figure 3 and Table 4).

Alkyne functionalized probes (*S*)-**3** and (*R*)-**3** (pEC_{50} = 7.51 and 7.22, respectively) have shown superior potency in comparison to free amines (*S*)-**1** and (*R*)-**1** (pEC_{50} = 6.72 and 6.80, respectively). Control agonist HU-210 and inverse agonist SR-144,528 demonstrated potency consistent with previously reported [^{35}S]-GTPγS binding assay values, further validating the experimental results (pEC_{50} = 8.83 and 8.23, respectively).[21,47] With respect to efficacy (E_{max}), probes (*S*)-**1**, (*R*)-**1**, (*S*)-**3**, and (*R*)-**3** induced functional response between –21.1 and –29.8%. Remarkably, comparison of the effect elicited by (*S*)-**1** in the cAMP and Gi-CASE assays (pEC_{50} = 5.57 and 6.72, respectively) suggests 14-fold increased potency of G protein recruitment over adenylyl cyclase inhibition, a striking bias within a CB_2R–Gα_i mediated pathway.

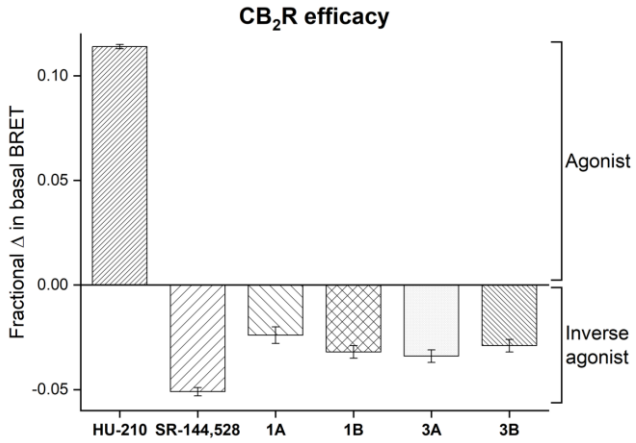

Figure 3. BRET-based Gi-CASE membrane assay to characterize G protein recruitment at CB_2R. Efficacy, E_{max}, of the compounds is shown as mean ± SEM, N = 3–4.

Table 4. Functional Characterization of G Protein Recruitment at CB_2R in a BRET Gi-CASE Assay‡

Probe	pEC_{50}	E_{max}/ %
(*S*)-**1**	6.72 ± 0.08	–21.1 ± 3.51
(*R*)-**1**	6.80 ± 0.18	–28.1 ± 2.63
(*S*)-**3**	7.51 ± 0.08	–29.8 ± 2.63
(*R*)-**3**	7.22 ± 0.32	–25.4 ± 2.63
SR-144,528	8.23 ± 0.05	–44.7 ± 1.75

‡Potency (pEC_{50}) and E_{max} data were obtained in a Gi-CASE BRET-based assay using membrane preparations from hCB_2R-HEK293 T-REx cells. Data were normalized to agonist HU-210 response (100%) and basal level (0%). Data are shown as mean ± SEM, N = 3–4.

Among the best studied G protein-independent signaling pathways of CB_2R is the β-arrestin cascade. β-Arrestins bind activated CB_2R following receptor phosphorylation, block further G protein mediated signaling, and destine the receptor for internalization.[15b] Representative compounds were profiled for β-arrestin recruitment in a BRET assay where an increase of the BRET ratio corresponds to recruitment of β-arrestin. In the assay (*S*)-**1**, (*R*)-**1**, (*S*)-**3**, and (*R*)-

3 demonstrated baseline BRET signal (Figure 4). In contrast, control agonists HU-308 and HU-210 showed expected recruitment of β-arrestin to CB_2R as indicated by increase in BRET intensity (pEC_{50} = 8.37 and 10.0, respectively). These results imply that none of the probes (*S*)-**1**, (*R*)-**1**, (*S*)-**3**, and (*R*)-**3** activate CB_2R toward β-arrestin recruitment.

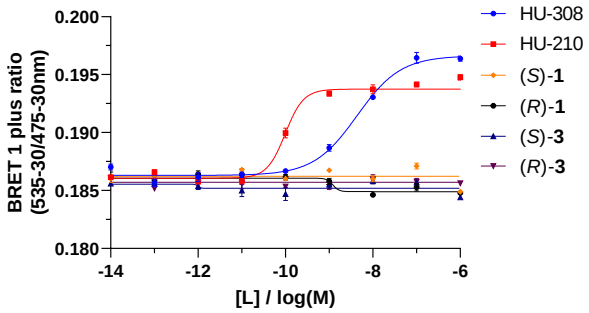

Figure 4. BRET-based assay to characterize β-arrestin recruitment at CB_2R. L = ligand.

Live Cell Pharmacological Profiling

Phosphorylation of ERK

Activation of CB_2R is associated with downstream stimulation of mitogen-activated protein kinases, such as $ERK_{1/2}$, mediated either via Gβγ or β-arrestins.[48] We have tested representative high-affinity fluorescent probe (*R*)-**2** for CB_2R-mediated phosphorylation of endogenous $ERK_{1/2}$ in a CB_2R inducible breast cancer HCC1954 cell line using the AlphaScreen *SureFire* phospho-ERK assay (Figure 5). Expression of CB_2R was optionally induced with doxycycline (DOX), and after 24 h the cells were incubated with a vehicle (0.1% DMSO), CB_2R selective agonist JWH133[49] (1 μM), or (*R*)-**2** (1 μM) for 30 min. Following cell lysis, lysates were incubated with a mixture containing donor and acceptor beads for 2 h at room temperature and the luminescence emission signal was measured.

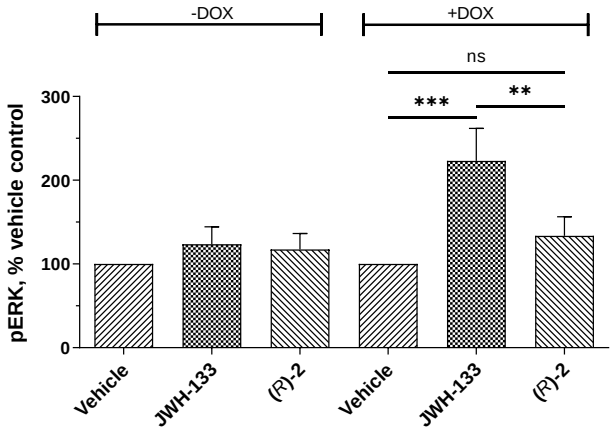

Figure 5. Live cell AlphaScreen *SureFire* phospho-ERK assay with CB_2R inducible breast cancer HCC1954 cell line. Cells were optionally induced with doxycycline (DOX) for 24 h to stimulate expression of CB_2R followed by incubation with a vehicle (0.1% DMSO), agonist JWH133[49] (1 μM) or (*R*)-**2** (1 μM) for 30 min. Statistical

significance was examined by one-way ANOVA followed by Tukey's *post hoc* test. ns = non-significant, ** $p < 0.01$, *** $p < 0.001$.

In the absence of CB_2R expression inducer (DOX) the phosphorylation levels of $ERK_{1/2}$ remained the same for cells treated with a vehicle, agonist JWH133, and (*R*)-**2**. In cells induced with DOX (1 μg/mL) to express CB_2R, JWH133 effectively stimulated $ERK_{1/2}$ phosphorylation mediated by CB_2R activation, in agreement with previously reported findings.[50] Addition of (*R*)-**2** had no effect on the level of phosphorylated $ERK_{1/2}$, which remained the same as for a vehicle. Data of the phospho-ERK cellular assay imply that (*R*)-**2** does not induce phosphorylation of $ERK_{1/2}$ by either CB_2R mediated Gβγ or β-arrestin signaling (or by non-CB_2R mediated pathways).

Ca^{2+} Signaling

Upon activation of CB_2R, Ca^{2+} is often released from intracellular reservoirs.[51] Our previous work reported that HU-308 and its photoswitchable derivative, *azo*-HU-308, increase intracellular Ca^{2+} in the mouse AtT-20 cell line.[27] Naturally, we were intrigued to investigate the response elicited by a representative probe. Epimeric mixture (*S*)-**3**/(*R*)-**3** was chosen as it allowed to avoid fluorophore interference with the Ca^{2+} dye, Fluo-4AM, and test both diastereomers simultaneously.

Rat isoform CB_2R-overexpressing AtT-20 cells [AtT-20(rCB2)] were infused with Fluo-4AM Ca^{2+} dye and imaged by real-time confocal microscopy (Figure 6). Addition of (*S*)-**3**/(*R*)-**3** (20 μM) did not elicit any increase in Fluo-4AM fluorescence, whereas subsequent addition of agonist HU-308 (20 μM) triggered a robust fluorescence response. Ionomycin was added at the end of the experiment to saturate Ca^{2+} levels. The results imply that neither (*S*)-**3** nor (*R*)-**3** mediate Ca^{2+} release by CB_2R activation and suggest that (*S*)-**3** and (*R*)-**3** can be rapidly displaced by HU-308.

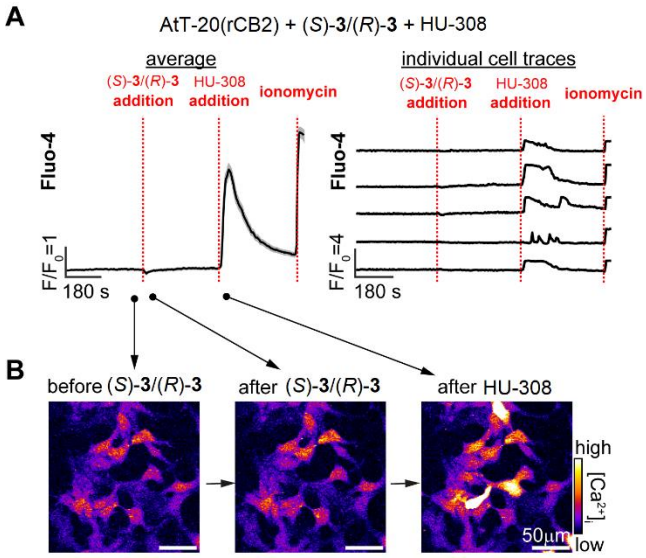

Figure 6. Live cell fluorescent Ca^{2+} imaging in rat CB_2R overexpressing AtT-20 cells (AtT-20(rCB2)) with Fluo-4AM (2 µM). After initial equilibration, (*S*)-**3**/(*R*)-**3** (20 µM) was added, followed by HU-308 (20 µM), and ionomycin (10 µM). Shown is the average response of 200 cells (**A**, left) and individual traces of five representative cells (**A**, right). Representative fluorescence images from different timepoints (**B**). Averaged data plotted as mean ± SEM, $N = 4$.

Fluorescence Confocal Microscopy in Live Cells

Having validated that the probes do not trigger CB_2R signaling, we proceeded to employ (*R*)-**7** and (*R*)-**9** in visualizing CB_2R by confocal fluorescence microscopy. Probes (*R*)-**7** and (*R*)-**9** were selected due to their bright, photostable, and extensively applied fluorophores Alexa488 and Alexa647. Additionally, the green- and red-shifted fluorescence spectra of (*R*)-**7** and (*R*)-**9** provide flexibility and potential for synergy with additional fluorescent proteins and small molecule dyes in multiplex imaging studies. Since many cannabinoid ligands tend to accumulate in plasma membranes due to their lipophilic nature, we set out to inspect whether (*R*)-**7** and (*R*)-**9** specifically label CB_2R in live cells.

First, AtT-20 cells stably expressing *N*-terminal SNAP-tagged human CB_2R [AtT-20(SNAP-hCB2)] were co-incubated with (*R*)-**7**, Janelia Fluor SNAP-549i (JF549i), and Hoechst33342 to label CB_2R, SNAP-tags, and nuclei, respectively. Confocal microscopy revealed bright fluorescence of Alexa488 and JF549i delineating the plasma membranes of AtT-20 cells (Figure 7A). Analysis of the corresponding intensity plot showed virtually identical co-localization overlap between the Alexa488 ((*R*)-**7**) and JF549i (SNAP-hCB_2R) signals (Figure 7B).

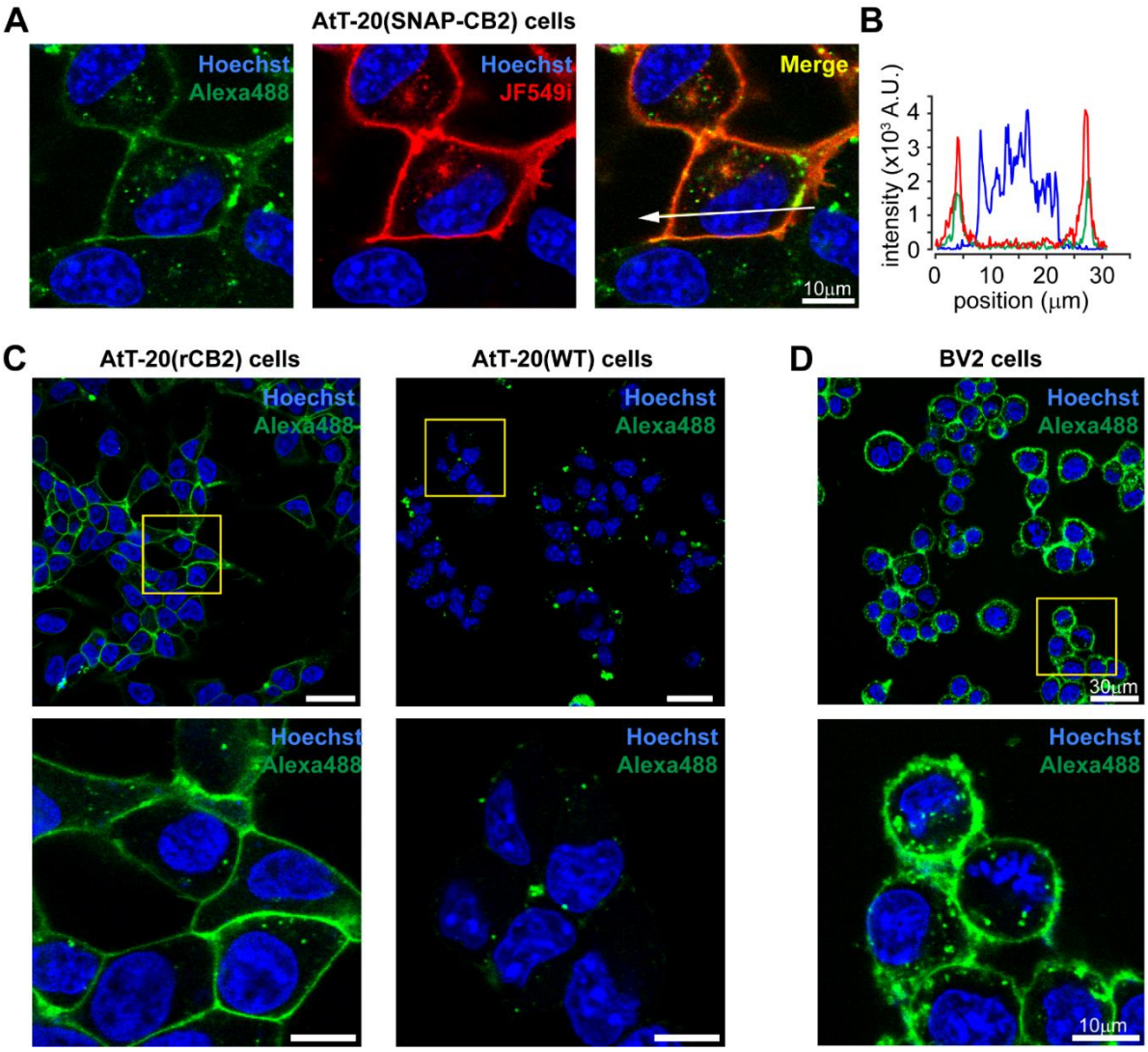

Figure 7. Confocal imaging of (*R*)-**7** in live cell lines; (**A**) AtT-20(SNAP-hCB2) cells were labelled for 15 min with (*R*)-**7** (Alexa488, 625 nM, green), SNAP-JF549i (JF549i, 500 nM, red), and Hoechst33342 (1 μM, blue) to visualize CB_2R, SNAP-tags, and nuclei, respectively. (**B**) Fluorescence intensity profiles across the white line for Alexa488, JF549i, and Hoechst33342. (**C**) AtT-20(rCB_2R) cells (left) and AtT-20 WT cells (right) were treated with (*R*)-**7** (625 nM, green) and Hoechst33342 (1 μM, blue) for 15 min and imaged by confocal microscopy. (**D**) Live BV-2 microglial cells that endogenously express CB_2R were incubated with (*R*)-**7** (2.5 μM, green) and Hoechst33342 (1 μM, blue) for 15 min and imaged by confocal microscopy.

Specificity of (*R*)-**7** for CB_2R was further ascertained by comparison of the response elicited in rat CB_2R isoform (rCB_2R)-expressing AtT-20 and wild-type (WT) cells, which do not express CB_2R.[52] AtT-20(rCB2) and AtT-20 WT cells were incubated with (*R*)-**7** and Hoechst33342 and studied by confocal imaging. Robust Alexa488 fluorescence signal was detected at the plasma membrane of AtT-20(rCB2) cells (Figure 7C, left). In stark contrast, AtT-20 WT cells showed only residual background fluorescence with no signal stemming from the cellular membrane (Figure 7C, right). Collectively, these results confirm that (*R*)-**7** specifically labels CB_2R at the plasma membrane.

Finally, the promising results with (*R*)-**7** in cells overexpressing CB_2R encouraged us to examine imaging CB_2R at naturally expressed levels. To this end, murine derived BV-2 cell line was selected due to its extensive use as a high fidelity, primary microglia culture model[53] that was applied in the study of neurodegeneration and neuroinflammation.[54] Importantly, BV-2 cells endogenously express CB_2R.[55] Following incubation of BV-2 cells with (*R*)-**7** and Hoechst33342, intense Alexa488 signal was observed at the plasma membrane across BV-2 cells (Figure 7D). These results highlight the use of (*R*)-**7** to visualize CB_2R at endogenous expression levels. Importantly, when (*R*)-**9** (Alexa647) was subject to analogous experiments it demonstrated equally outstanding specificity for CB_2R in AtT-20 cells (see SI Figure S2ABC) combined with strong signal intensity in the BV-2 microglial cell line (see SI Figure S2D). Finally, the data imply that performance of (*R*)-**7** and (*R*)-**9** remains uncompromised by interspecies differences and the probes can be employed to investigate both human and murine isoforms of CB_2R.

Molecular Dynamics Simulations Unravel Pharmacophore Determinants of Receptor Activation

Molecular dynamics (MD) studies were performed in a membrane environment with inverse agonists (*S*)-**3**, (*R*)-**3** and their agonist counterpart **ago-3** to contrast their interactions with CB_2R at a molecular level and elucidate their orthogonal functional profiles. To this end, X-ray structure of CB_2R in an inactive state in complex with AM10257 (PDB:5ZTY) was selected as a starting point for 1 μs MD simulations to assess ligand stability and identify rearrangements within the binding site.

All three ligands adopt an L-shape conformation with the pendant alkyl chain hosted in a cleft formed by $Phe183^{ECL2}$, $Tyr190^{5.39}$, $Trp194^{5.43}$, and $Thr114^{3.33}$ (see Figure 8 and SI Figures S3 and S4). The resorcinol engages in π–π interactions with $Phe183^{ECL2}$ while the pinene core is surrounded by aromatic residues ($Phe183^{ECL2}$, $Phe91^{2.61}$, and $Phe94^{2.64}$). An rmsd plot of **ago-3** following a best fit of protein backbone shows an initial rearrangement followed by a periodic 'breathing-like' motion of the resorcinol and alkyl chain that oscillate between bent and flat conformations (see SI Figures S3 and S5). Furthermore, in accord with our earlier work,[28] in the CB_2R–**ago-3** complex the amide group of **ago-3** forms a stable hydrogen bond with the carbonyl of $Ser90^{2.60}$.

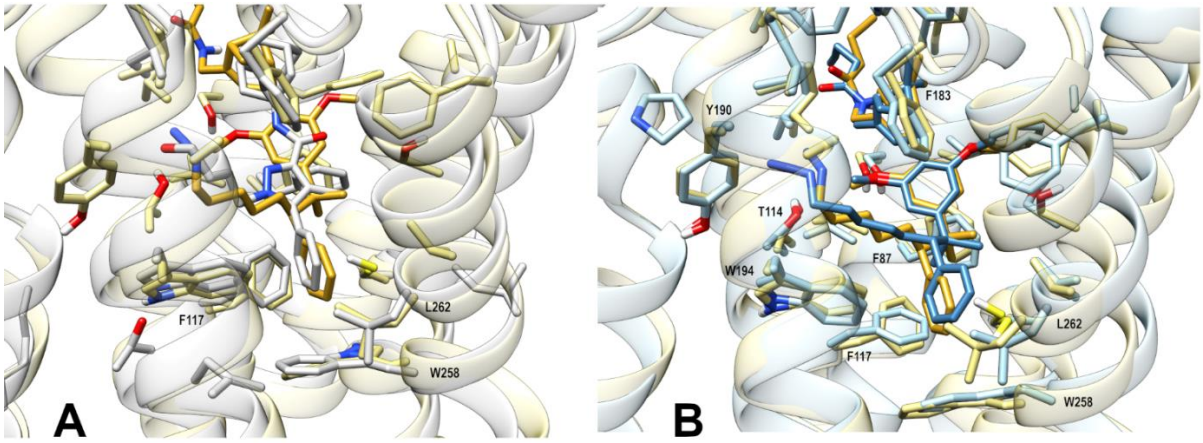

Figure 8. Representative frames from molecular dynamics (MD) simulations of CB_2R (PDB:5ZTY) in complex with (*S*)-**3** or (*R*)-**3**; Superimposition at level of protein backbone of (**A**) CB_2R X-ray structure with AM10257 (light grey) and (*R*)-**3** MD complex (ligand in gold and protein in light yellow) and of (**B**) the two inverse agonist complexes (*S*)-**3** (ligand in blue and protein light blue) and (*R*)-**3** (ligand in gold and protein in light yellow).

In agreement with the in silico docking (Figure 1) the MD simulations suggest the C(2') phenyl rings of (*S*)-**3** and (*R*)-**3** mirror that of AM10257 and engage in π–π contacts with Phe117$^{3.36}$ and Trp258$^{6.48}$ (see Figure 8A and SI Figure S6). In contrast to **ago-3**, no initial rearrangement in the binding poses of (*S*)-**3** and (*R*)-**3** was observed in their rmsd plots (see SI Figure S7). Ligands (*S*)-**3** and (*R*)-**3** share similar binding modes of the pinene-resorcinol core, however, significant differences are observed in the orientation adopted by *gem*-dimethyl groups and the C(2') phenyl rings (see Figure 8B and SI Figure S8). In particular, the *gem*-dimethyl group of (*S*)-**3** is rotated clockwise compared to that of (*R*)-**3** and the C(2') phenyl of (*S*)-**3** is rotated toward Leu262$^{6.44}$, inducing a minor displacement of helix H6, while that of (*R*)-**3** protrudes deeper toward Trp258$^{6.48}$. In both cases the conformation of the Trp258$^{6.48}$ toggle switch is restricted and CB_2R thus stabilized in its inactive state, in stark contrast to the interactions observed with the agonist complex.

Superimposition of CB_2R protein backbone employing the X-ray structure with AM10257 and the representative MD frames in complex with either (*S*)-**3** (see SI Figure S6) or (*R*)-**3** (Figure 8A) imply that (*R*)-**3** more closely resembles the binding mode of AM10257 in the crystallized complex. In particular, the secondary binding pocket featuring Trp258$^{6.48}$ and the surrounding residues Phe117$^{3.36}$ and Leu262$^{6.44}$ are in an excellent agreement between AM10257 and (*R*)-**3**.

Finally, the difference in free energy of binding (ΔΔG) was determined for (*R*)-**3** and (*S*)-**3** using molecular mechanics/Poisson–Boltzmann (Generalized Born) surface area (MM/PB(GB)SA) calculations (see SI Table S1). The data

imply that binding of (*R*)-**3** is more stable by –0.76 kcal mol^{-1} (MM/GBSA) and –0.40 kcal mol^{-1} (MM/PBSA) in comparison to (*S*)-**3**. Notably, the calculated ΔΔGs are in agreement with the experimental difference in ΔΔG = –0.9 kcal mol^{-1} for epimers (*S*)-**3** and (*R*)-**3**.

CONCLUSION

This study describes the in silico guided structure-based transformation of functionality from agonist to inverse agonist of HU-308, a ligand extensively applied to unravel CB_2R pharmacology and currently investigated in clinical trials. The novel inverse agonist platform ligands (*S*)-**1** and (*R*)-**1** demonstrated high binding affinity for CB_2R and selectivity against CB_1R that was retained upon functionalization with a range of chemically distinct substituents and fluorophores. The functional response exerted on CB_2R by (*S*)-**1**, (*R*)-**1**, and their derivatives was evaluated by HTRF and BRET and implied an inverse agonist profile in cAMP as well as G protein recruitment assays, and no induction of β-arrestin–receptor association. Live cell experiments with (*R*)-**2** and (*S*)-**3**/(*R*)-**3** demonstrated that the probes do not activate CB_2R toward $ERK_{1/2}$ phosphorylation and Ca^{2+} release, respectively. Confocal fluorescence microscopy experiments with (*R*)-**7** and (*R*)-**9** in AtT-20 cells expressing human and rat CB_2R isoforms demonstrated excellent target specificity and species translatability. Treatment of BV-2 microglial cell line with (*R*)-**7** and (*R*)-**9** allowed imaging of CB_2R at endogenously expressed levels in live cells. Finally, MD simulations with (*S*)-**3,** (*R*)-**3**, and **ago-3** corroborate the critical role of the C(2') phenyl substituent in conferring the functional profile by modulating the CB_2R toggle switch $Trp258^{6.48}$ of the CWxP motif.

To the best of our knowledge, this work discloses the first discovery of a ligand platform for CB_2R that retains its inverse agonist functional profile, exceptional affinity, and selectivity independent of its conjugation to a range of diverse functional groups. The probes introduce a long sought-after complementarity to an agonist-dominated toolkit to study, elucidate, and unlock the full therapeutic potential of CB_2R. Moreover, the platform ligands promise broad application and synergy with previously published work which awaited discovery of an inverse agonist.[14a] The exponential rise in resolved structures of class A GPCRs, many of which are available in inactive, intermediate, and fully active states, has enabled unprecedented insight into the mechanism of receptor activation.[35,56] Thus, the logic and experimental framework disclosed herein may

aid in the structure-based design of agonists, antagonists, and inverse agonists for GPCRs beyond CB_2R.

CONFLICT OF INTEREST

The authors declare the following competing financial interest: M.K., R.C.S., B.K., W.G., U.G., and E.M.C have filed a patent on CB_2R selective modulators and fluorescent probes.

CORRESPONDING AUTHORS

*E-mail: erickm.carreira@org.chem.ethz.ch
*E-mail: uwe.grether@roche.com
*E-mail: frankja@ohsu.edu

ACKNOWLEDGMENTS

We thank Eric Bald for his help with chiral separations and Isabelle Kaufmann for her assistance with logistics and administration. We are grateful to Dr. Raphael Bigler, Dr. Paolo Tosatti, Dr. Stephan Bachmann, Dr. Kurt Püntener, and Manuela Müller for their expertise, insight and experimental help with high-pressure hydrogenations. We thank René Arnold, Rainer Frankenstein, and Stephan Burkhardt for their help with NMR measurements, and Jan Kovacovic for his expertise with high pressure hydrogenation, and the MoBiAS team for MS analysis. We are grateful to Dr. Nils Trapp and Michael Solar for X-ray crystallographic analysis. M.K. and R.C.S. gratefully acknowledge a fellowship by the Scholarship Fund of the Swiss Chemical Industry (SSCI). MD studies have been funded by project code PIR01_00011 "IBISCo", PON 2014-2020. We would like to thank Prof. Dr. Jürg Gertsch (University of Bern, Switzerland) for kindly providing the CB_2R expressing cells. Research in the laboratory of C.W.G has been supported by the Austrian Science Fund (FWF) through project P32109. N.T has been supported by a short-term scientific mission (STSM) grant from the EU COST Action CA 18133 (ERNEST). T.H. has been supported by the National Key Research and Development Program of China grant 2022YFA1302903.

REFERENCES

1. Maccarrone, M. *New Tools to Interrogate Endocannabinoid Signalling: From Natural Compounds to Synthetic Drugs*; The Royal Society of Chemistry, 2021.
2. Munro, S.; Thomas, K. L.; Abu-Shaar, M. Molecular characterization of a peripheral receptor for cannabinoids. *Nature* **1993**, *365*, 61-65
3. Goncalves, E. D.; Dutra, R. C. Cannabinoid receptors as therapeutic targets for autoimmune diseases: where do we stand? *Drug Discovery Today* **2019**, *24*, 1845-1853
4. Rossi, F.; Punzo, F.; Umano, G. R.; Argenziano, M.; Miraglia Del Giudice, E. Role of Cannabinoids in Obesity. *Int. J. Mol. Sci.* **2018**, *19*, 2690-2700
5. Kumawat, V. S.; Kaur, G. Therapeutic potential of cannabinoid receptor 2 in the treatment of diabetes mellitus and its complications. *Eur. J. Pharmacol.* **2019**, *862*, 172628-172633
6. Shang, Y.; Tang, Y. The central cannabinoid receptor type-2 (CB2) and chronic pain. *Int. J. Neurosci.* **2017**, *127*, 812-823
7. Khan, H.; Ghori, F. K.; Ghani, U.; Javed, A.; Zahid, S. Cannabinoid and endocannabinoid system: a promising therapeutic intervention for multiple sclerosis. *Mol. Biol. Rep.* **2022**, *49*, 5117-5131
8. Laezza, C.; Pagano, C.; Navarra, G.; Pastorino, O.; Proto, M. C.; Fiore, D.; Piscopo, C.; Gazzerro, P.; Bifulco, M. The Endocannabinoid System: A Target for Cancer Treatment. *Int. J. Mol. Sci.* **2020**, *21*, 747-767
9. Zhou, L.; Zhou, S.; Yang, P.; Tian, Y.; Feng, Z.; Xie, X. Q.; Liu, Y. Targeted inhibition of the type 2 cannabinoid receptor is a novel approach to reduce renal fibrosis. *Kidney Int.* **2018**, *94*, 756-772
10. Lunn, C. A.; Reich, E. P.; Fine, J. S.; Lavey, B.; Kozlowski, J. A.; Hipkin, R. W.; Lundell, D. J.; Bober, L. Biology and therapeutic potential of cannabinoid CB2 receptor inverse agonists. *Br. J. Pharmacol.* **2008**, *153*, 226-239
11. Reiner, A.; Heldt, S. A.; Presley, C. S.; Guley, N. H.; Elberger, A. J.; Deng, Y.; D'Surney, L.; Rogers, J. T.; Ferrell, J.; Bu, W.; Del Mar, N.; Honig, M. G.; Gurley, S. N.; Moore, B. M. Motor, visual and emotional deficits in mice after closed-head mild traumatic brain injury are alleviated by the novel CB2 inverse agonist SMM-189. *Int. J. Mol. Sci.* **2014**, *16*, 758-787
12. Bu, W.; Ren, H.; Deng, Y.; Del Mar, N.; Guley, N. M.; Moore, B. M.; Honig, M. G.; Reiner, A. Mild Traumatic Brain Injury Produces Neuron Loss That Can Be Rescued by Modulating Microglial Activation Using a CB2 Receptor Inverse Agonist. *Front. Neurosci.* **2016**, *10*, 449-465

13. Alghamdi, S. S.; Mustafa, S. M.; Moore Ii, B. M. Synthesis and biological evaluation of a ring analogs of the selective CB2 inverse agonist SMM-189. *Bioorg. Med. Chem. Lett.* **2021**, *33*, 116035-116051
14. A Study to Investigate the Efficacy and Safety of RG7774 in Patients With Diabetes Mellitus Type 1 or Type 2 With Treatment-Naive Diabetic Retinopathy (CANBERRA), https://classic.clinicaltrials.gov/ct2/show/NCT04265261, (accessed September 19, 2023).
15. Whiting, Z. M.; Yin, J.; de la Harpe, S. M.; Vernall, A. J.; Grimsey, N. L. Developing the Cannabinoid Receptor 2 (CB2) pharmacopoeia: past, present, and future. *Trends Pharmacol Sci* **2022**, *43*, 754-771
16. Brownjohn, P. W.; Ashton, J. C. Spinal cannabinoid CB2 receptors as a target for neuropathic pain: an investigation using chronic constriction injury. *Neuroscience* **2012**, *203*, 180-193
17. Cecyre, B.; Thomas, S.; Ptito, M.; Casanova, C.; Bouchard, J. F. Evaluation of the specificity of antibodies raised against cannabinoid receptor type 2 in the mouse retina. *Naunyn-Schmiedeberg's Arch. Pharmacol.* **2014**, *387*, 175-184
18. Marchalant, Y.; Brownjohn, P. W.; Bonnet, A.; Kleffmann, T.; Ashton, J. C. Validating Antibodies to the Cannabinoid CB2 Receptor: Antibody Sensitivity Is Not Evidence of Antibody Specificity. *J. Histochem. Cytochem.* **2014**, *62*, 395-404
19. Zhang, H. Y.; Shen, H.; Jordan, C. J.; Liu, Q. R.; Gardner, E. L.; Bonci, A.; Xi, Z. X. CB2 receptor antibody signal specificity: correlations with the use of partial CB2-knockout mice and anti-rat CB2 receptor antibodies. *Acta Pharmacol. Sin.* **2019**, *40*, 398-409
20. Chen, D. J.; Gao, M.; Gao, F. F.; Su, Q. X.; Wu, J. Brain cannabinoid receptor 2: expression, function and modulation. *Acta Pharmacol. Sin.* **2017**, *38*, 312-316
21. Kosar, M.; Sykes, D. A.; Viray, A. E. G.; Vitale, R. M.; Sarott, R. C.; Ganzoni, R. L.; Onion, D.; Tobias, J. M.; Leippe, P.; Ullmer, C.; Zirwes, E. A.; Guba, W.; Grether, U.; Frank, J. A.; Veprintsev, D. B.; Carreira, E. M. Platform Reagents Enable Synthesis of Ligand-Directed Covalent Probes: Study of Cannabinoid Receptor 2 in Live Cells. *J. Am. Chem. Soc.* **2023**, *145*, 15094-15108
22. Gazzi, T.; Brennecke, B.; Atz, K.; Korn, C.; Sykes, D.; Forn-Cuni, G.; Pfaff, P.; Sarott, R. C.; Westphal, M. V.; Mostinski, Y.; Mach, L.; Wasinska-Kalwa, M.; Weise, M.; Hoare, B. L.; Miljuš, T.; Mexi, M.; Roth, N.; Koers, E. J.; Guba, W.; Alker, A.; Rufer, A. C.; Kusznir, E. A.; Huber, S.; Raposo, C.; Zirwes, E. A.; Osterwald, A.; Pavlovic, A.; Moes, S.; Beck, J.; Nettekoven, M.; Benito-Cuesta, I.; Grande, T.; Drawnel, F.; Widmer, G.; Holzer, D.; van der Wel, T.; Mandhair, H.; Honer, M.; Fingerle, J.; Scheffel, J.; Broichhagen, J.; Gawrisch, K.; Romero, J.; Hillard, C. J.; Varga, Z. V.; van der Stelt, M.; Pacher, P.; Gertsch, J.; Ullmer, C.; McCormick, P. J.; Oddi, S.; Spaink, H. P.;

Maccarrone, M.; Veprintsev, D. B.; Carreira, E. M.; Grether, U.; Nazaré, M. Detection of cannabinoid receptor type 2 in native cells and zebrafish with a highly potent, cell-permeable fluorescent probe. *Chem. Sci.* **2022**, *13*, 5539-5545
23. Sarott, R. C.; Westphal, M. V.; Pfaff, P.; Korn, C.; Sykes, D. A.; Gazzi, T.; Brennecke, B.; Atz, K.; Weise, M.; Mostinski, Y.; Hompluem, P.; Koers, E.; Miljus, T.; Roth, N. J.; Asmelash, H.; Vong, M. C.; Piovesan, J.; Guba, W.; Rufer, A. C.; Kusznir, E. A.; Huber, S.; Raposo, C.; Zirwes, E. A.; Osterwald, A.; Pavlovic, A.; Moes, S.; Beck, J.; Benito-Cuesta, I.; Grande, T.; Ruiz de Marti, N. E. S.; Yeliseev, A.; Drawnel, F.; Widmer, G.; Holzer, D.; van der Wel, T.; Mandhair, H.; Yuan, C. Y.; Drobyski, W. R.; Saroz, Y.; Grimsey, N.; Honer, M.; Fingerle, J.; Gawrisch, K.; Romero, J.; Hillard, C. J.; Varga, Z. V.; van der Stelt, M.; Pacher, P.; Gertsch, J.; McCormick, P. J.; Ullmer, C.; Oddi, S.; Maccarrone, M.; Veprintsev, D. B.; Nazare, M.; Grether, U.; Carreira, E. M. Development of High-Specificity Fluorescent Probes to Enable Cannabinoid Type 2 Receptor Studies in Living Cells. *J. Am. Chem. Soc.* **2020**, *142*, 16953-16964
24. Grimsey, N. L.; Goodfellow, C. E.; Dragunow, M.; Glass, M. Cannabinoid receptor 2 undergoes Rab5-mediated internalization and recycles via a Rab11-dependent pathway. *Biochim. Biophys. Acta* **2011**, *1813*, 1554-1560
25. Chen, X.; Zheng, C.; Qian, J.; Sutton, S. W.; Wang, Z.; Lv, J.; Liu, C.; Zhou, N. Involvement of beta-arrestin-2 and clathrin in agonist-mediated internalization of the human cannabinoid CB2 receptor. *Curr. Mol. Pharmacol.* **2014**, *7*, 67-80
26. Weis, W. I.; Kobilka, B. K. The Molecular Basis of G Protein-Coupled Receptor Activation. *Annu. Rev. Biochem* **2018**, *87*, 897-919
27. Cooper, A. G.; MacDonald, C.; Glass, M.; Hook, S.; Tyndall, J. D. A.; Vernall, A. J. Alkyl indole-based cannabinoid type 2 receptor tools: Exploration of linker and fluorophore attachment. *Eur. J. Med. Chem.* **2018**, *145*, 770-789
28. Sexton, M.; Woodruff, G.; Horne, E. A.; Lin, Y. H.; Muccioli, G. G.; Bai, M.; Stern, E.; Bornhop, D. J.; Stella, N. NIR-mbc94, a fluorescent ligand that binds to endogenous CB(2) receptors and is amenable to high-throughput screening. *Chem Biol* **2011**, *18*, 563-8
29. Singh, S.; Oyagawa, C. R. M.; Macdonald, C.; Grimsey, N. L.; Glass, M.; Vernall, A. J. Chromenopyrazole-based High Affinity, Selective Fluorescent Ligands for Cannabinoid Type 2 Receptor. *ACS Med. Chem. Lett.* **2019**, *10*, 209-214
30. L. Hanus, A. B., S. Tchilibon, S. Shiloah, D. Goldenberg, M. Horowitz, R. G. Pertwee, R. A. Ross, R. Mechoulam, E. Fride HU-308: A specific agonist for CB2, a peripheral cannabinoid receptor. *Proc. Natl. Acad. Sci. U. S. A.* **1999**, *96*, 14228-14233
31. Soethoudt, M.; Grether, U.; Fingerle, J.; Grim, T. W.; Fezza, F.; de Petrocellis, L.; Ullmer, C.; Rothenhausler, B.; Perret, C.; van Gils, N.; Finlay, D.; MacDonald, C.; Chicca, A.; Gens, M. D.; Stuart, J.; de Vries, H.;

Mastrangelo, N.; Xia, L.; Alachouzos, G.; Baggelaar, M. P.; Martella, A.; Mock, E. D.; Deng, H.; Heitman, L. H.; Connor, M.; Di Marzo, V.; Gertsch, J.; Lichtman, A. H.; Maccarrone, M.; Pacher, P.; Glass, M.; van der Stelt, M. Cannabinoid CB2 receptor ligand profiling reveals biased signalling and off-target activity. *Nat. Commun.* **2017**, *8*, 13958-13972
32. LaBuda, C. J.; Koblish, M.; Little, P. J. Cannabinoid CB2 receptor agonist activity in the hindpaw incision model of postoperative pain. *Eur. J. Pharmacol.* **2005**, *527*, 172-174
33. Ossola, C. A.; Surkin, P. N.; Mohn, C. E.; Elverdin, J. C.; Fernandez-Solari, J. Anti-Inflammatory and Osteoprotective Effects of Cannabinoid-2 Receptor Agonist HU-308 in a Rat Model of Lipopolysaccharide-Induced Periodontitis. *J. Periodontol.* **2016**, *87*, 725-734
34. Rentsch, P.; Stayte, S.; Egan, T.; Clark, I.; Vissel, B. Targeting the cannabinoid receptor CB2 in a mouse model of l-dopa induced dyskinesia. *Neurobiol. Dis.* **2020**, *134*, 104646-104659
35. Espejo-Porras, F.; Garcia-Toscano, L.; Rodriguez-Cueto, C.; Santos-Garcia, I.; de Lago, E.; Fernandez-Ruiz, J. Targeting glial cannabinoid CB(2) receptors to delay the progression of the pathological phenotype in TDP-43 (A315T) transgenic mice, a model of amyotrophic lateral sclerosis. *Br. J. Pharmacol.* **2019**, *176*, 1585-1600
36. Tetra Bio-Pharma. ARDS-003, https://tetrabiopharma.com/pipeline/ (accessed September 19, 2023).
37. Sarott, R. C.; Viray, A. E. G.; Pfaff, P.; Sadybekov, A.; Rajic, G.; Katritch, V.; Carreira, E. M.; Frank, J. A. Optical Control of Cannabinoid Receptor 2-Mediated Ca(2+) Release Enabled by Synthesis of Photoswitchable Probes. *J. Am. Chem. Soc.* **2021**, *143*, 736-743
38. Westphal, M. V.; Sarott, R. C.; Zirwes, E. A.; Osterwald, A.; Guba, W.; Ullmer, C.; Grether, U.; Carreira, E. M. Highly Selective, Amine-Derived Cannabinoid Receptor 2 Probes. *Chem. Eur. J.* **2020**, *26*, 1380-1387
39. Lee, J.; Schapira, M. The Promise and Peril of Chemical Probe Negative Controls. *ACS Chem. Biol.* **2021**, *16*, 579-585
40. Bunnage, M. E.; Chekler, E. L.; Jones, L. H. Target validation using chemical probes. *Nat. Chem. Biol.* **2013**, *9*, 195-199
41. Congreve, M.; de Graaf, C.; Swain, N. A.; Tate, C. G. Impact of GPCR Structures on Drug Discovery. *Cell* **2020**, *181*, 81-91
42. Olivella, M.; Caltabiano, G.; Cordomi, A. The role of Cysteine 6.47 in class A GPCRs. *BMC Struct. Biol.* **2013**, *13*, 3
43. Hauser, A. S.; Attwood, M. M.; Rask-Andersen, M.; Schioth, H. B.; Gloriam, D. E. Trends in GPCR drug discovery: new agents, targets and indications. *Nat. Rev. Drug Discovery* **2017**, *16*, 829-842
44. Li, X.; Chang, H.; Bouma, J.; de Paus, L. V.; Mukhopadhyay, P.; Paloczi, J.; Mustafa, M.; van der Horst, C.; Kumar, S. S.; Wu, L.; Yu, Y.; van den Berg, R.; Janssen, A. P. A.; Lichtman, A.; Liu, Z. J.; Pacher, P.; van der

Stelt, M.; Heitman, L. H.; Hua, T. Structural basis of selective cannabinoid CB(2) receptor activation. *Nat. Commun.* **2023**, *14*, 1447-1463
45. Li, X.; Hua, T.; Vemuri, K.; Ho, J. H.; Wu, Y.; Wu, L.; Popov, P.; Benchama, O.; Zvonok, N.; Locke, K.; Qu, L.; Han, G. W.; Iyer, M. R.; Cinar, R.; Coffey, N. J.; Wang, J.; Wu, M.; Katritch, V.; Zhao, S.; Kunos, G.; Bohn, L. M.; Makriyannis, A.; Stevens, R. C.; Liu, Z. J. Crystal Structure of the Human Cannabinoid Receptor CB2. *Cell* **2019**, *176*, 459-467
46. Zhou, Q.; Yang, D.; Wu, M.; Guo, Y.; Guo, W.; Zhong, L.; Cai, X.; Dai, A.; Jang, W.; Shakhnovich, E. I.; Liu, Z. J.; Stevens, R. C.; Lambert, N. A.; Babu, M. M.; Wang, M. W.; Zhao, S. Common activation mechanism of class A GPCRs. *eLife* **2019**, *8*,
47. Hua, T.; Li, X.; Wu, L.; Iliopoulos-Tsoutsouvas, C.; Wang, Y.; Wu, M.; Shen, L.; Brust, C. A.; Nikas, S. P.; Song, F.; Song, X.; Yuan, S.; Sun, Q.; Wu, Y.; Jiang, S.; Grim, T. W.; Benchama, O.; Stahl, E. L.; Zvonok, N.; Zhao, S.; Bohn, L. M.; Makriyannis, A.; Liu, Z. J. Activation and Signaling Mechanism Revealed by Cannabinoid Receptor-Gi Complex Structures. *Cell* **2020**, *180*, 655-665
48. Bow, E. W.; Rimoldi, J. M. The Structure-Function Relationships of Classical Cannabinoids: CB1/CB2 Modulation. *Perspect. Med. Chem.* **2016**, *8*, 17-39
49. John W. Huffman; Julia A. H. Lainton; W. Kenneth Banner; Sammy G. Duncan; Robert D. Jordan; Shu Yu, a. D. D.; Billy R. Martin; Jenny L. WiIey; Compton, D. R. Side chain methyl analogues of Δ8-THC. *Tetrahedron* **1997**, *53*, 1557-1576
50. Sharma, R.; Nikas, S. P.; Paronis, C. A.; Wood, J. T.; Halikhedkar, A.; Guo, J. J.; Thakur, G. A.; Kulkarni, S.; Benchama, O.; Raghav, J. G.; Gifford, R. S.; Jarbe, T. U.; Bergman, J.; Makriyannis, A. Controlled-deactivation cannabinergic ligands. *J. Med. Chem.* **2013**, *56*, 10142-10157
51. Corrie, J. E. T. Preparation and Properties of Unsymmetrical Benzoins and Related Compounds. *Tetrahedron* **1998**, *54*, 5407-5416
52. Zanato, C.; Pelagalli, A.; Marwick, K. F.; Piras, M.; Dall'Angelo, S.; Spinaci, A.; Pertwee, R. G.; Wyllie, D. J.; Hardingham, G. E.; Zanda, M. Synthesis, radio-synthesis and in vitro evaluation of terminally fluorinated derivatives of HU-210 and HU-211 as novel candidate PET tracers. *Org. Biomol. Chem.* **2017**, *15*, 2086-2096
53. Jiang, S.; Iliopoulos-Tsoutsouvas, C.; Tong, F.; Brust, C. A.; Keenan, C. M.; Raghav, J. G.; Hua, T.; Wu, S.; Ho, J. H.; Wu, Y.; Grim, T. W.; Zvonok, N.; Thakur, G. A.; Liu, Z. J.; Sharkey, K. A.; Bohn, L. M.; Nikas, S. P.; Makriyannis, A. Novel Functionalized Cannabinoid Receptor Probes: Development of Exceptionally Potent Agonists. *J. Med. Chem.* **2021**, *64*, 3870-3884

54. Bailey, W. F.; Punzalan, E. R. Convenient General Method for the Preparation of Primary Alkyllithiums by Lithium-Iodine Exchange. *J. Org. Chem.* **1990**, *55*, 5404-5406
55. Hoffmann, C.; Castro, M.; Rinken, A.; Leurs, R.; Hill, S. J.; Vischer, H. F. Ligand Residence Time at G-protein-Coupled Receptors-Why We Should Take Our Time To Study It. *Mol. Pharmacol.* **2015**, *88*, 552-560
56. Copeland, R. A. The drug-target residence time model: a 10-year retrospective. *Nat. Rev. Drug Discovery* **2016**, *15*, 87-95
57. Copeland, R. A.; Pompliano, D. L.; Meek, T. D. Drug-target residence time and its implications for lead optimization. *Nat. Rev. Drug Discovery* **2006**, *5*, 730-739
58. Sophocleous, A.; Landao-Bassonga, E.; Van't Hof, R. J.; Idris, A. I.; Ralston, S. H. The type 2 cannabinoid receptor regulates bone mass and ovariectomy-induced bone loss by affecting osteoblast differentiation and bone formation. *Endocrinology* **2011**, *152*, 2141-2149
59. Dhopeshwarkar, A.; Mackie, K. CB2 Cannabinoid receptors as a therapeutic target-what does the future hold? *Mol. Pharmacol.* **2014**, *86*, 430-437
60. Dhopeshwarkar, A.; Mackie, K. Functional Selectivity of CB2 Cannabinoid Receptor Ligands at a Canonical and Noncanonical Pathway. *J. Pharmacol. Exp. Ther.* **2016**, *358*, 342-351
61. Atwood, B. K.; Wager-Miller, J.; Haskins, C.; Straiker, A.; Mackie, K. Functional selectivity in CB(2) cannabinoid receptor signaling and regulation: implications for the therapeutic potential of CB(2) ligands. *Mol. Pharmacol.* **2012**, *81*, 250-263
62. Scott-Dennis, M.; Rafani, F. A.; Yi, Y.; Perera, T.; Harwood, C. R.; Guba, W.; Rufer, A. C.; Grether, U.; Veprintsev, D. B.; Sykes, D. A. Development of a membrane-based Gi-CASE biosensor assay for profiling compounds at cannabinoid receptors. *Front. Pharmacol.* **2023**, *14*,
63. Manera, C.; Malfitano, A. M.; Parkkari, T.; Lucchesi, V.; Carpi, S.; Fogli, S.; Bertini, S.; Laezza, C.; Ligresti, A.; Saccomanni, G.; Savinainen, J. R.; Ciaglia, E.; Pisanti, S.; Gazzerro, P.; Di Marzo, V.; Nieri, P.; Macchia, M.; Bifulco, M. New quinolone- and 1,8-naphthyridine-3-carboxamides as selective CB2 receptor agonists with anticancer and immuno-modulatory activity. *Eur. J. Med. Chem.* **2015**, *97*, 10-18
64. Bouaboula, M.; Poinot-Chazel, C.; Marchand, J.; Canat, X.; Bourrie, B.; Rinaldi-Carmona, M.; Calandra, B.; Le Fur, G.; Casellas, P. Signaling pathway associated with stimulation of CB2 peripheral cannabinoid receptor. Involvement of both mitogen-activated protein kinase and induction of Krox-24 expression. *Eur. J. Biochem.* **1996**, *237*, 704-711
65. Howlett, A. C.; Abood, M. E. CB1 and CB2 Receptor Pharmacology. *Adv. Pharmacol.* **2017**, *80*, 169-206
66. Huffman, J. W.; Liddle, J.; Yu, S.; Aung, M. M.; Abood, M. E.; Wiley, J. L.; Martin, B. R. 3-(1',1'-Dimethylbutyl)-1-deoxy-delta8-THC and related

compounds: synthesis of selective ligands for the CB2 receptor. *Biorg. Med. Chem.* **1999**, *7*, 2905-2914
67. Hashiesh, H. M.; Sharma, C.; Goyal, S. N.; Jha, N. K.; Ojha, S. Pharmacological Properties, Therapeutic Potential and Molecular Mechanisms of JWH133, a CB2 Receptor-Selective Agonist. *Front. Pharmacol.* **2021**, *12*, 702675
68. Zoratti, C.; Kipmen-Korgun, D.; Osibow, K.; Malli, R.; Graier, W. F. Anandamide initiates Ca(2+) signaling via CB2 receptor linked to phospholipase C in calf pulmonary endothelial cells. *Br. J. Pharmacol.* **2003**, *140*, 1351-1362
69. Juan-Pico, P.; Fuentes, E.; Bermudez-Silva, F. J.; Javier Diaz-Molina, F.; Ripoll, C.; Rodriguez de Fonseca, F.; Nadal, A. Cannabinoid receptors regulate Ca(2+) signals and insulin secretion in pancreatic beta-cell. *Cell Calcium* **2006**, *39*, 155-162
70. Brailoiu, G. C.; Deliu, E.; Marcu, J.; Hoffman, N. E.; Console-Bram, L.; Zhao, P.; Madesh, M.; Abood, M. E.; Brailoiu, E. Differential activation of intracellular versus plasmalemmal CB2 cannabinoid receptors. *Biochemistry* **2014**, *53*, 4990-4999
71. Atwood, B. K.; Lopez, J.; Wager-Miller, J.; Mackie, K.; Straiker, A. Expression of G protein-coupled receptors and related proteins in HEK293, AtT20, BV2, and N18 cell lines as revealed by microarray analysis. *BMC Genomics* **2011**, *12*, 14
72. Henn, A.; Lund, S.; Hedtjarn, M.; Schrattenholz, A.; Porzgen, P.; Leist, M. The suitability of BV2 cells as alternative model system for primary microglia cultures or for animal experiments examining brain inflammation. *ALTEX* **2009**, *26*, 83-94
73. Olajide, O. A.; Iwuanyanwu, V. U.; Adegbola, O. D.; Al-Hindawi, A. A. SARS-CoV-2 Spike Glycoprotein S1 Induces Neuroinflammation in BV-2 Microglia. *Molecular Neurobiology* **2022**, *59*, 445-458
74. Yao, K.; Zu, H. B. Microglial polarization: novel therapeutic mechanism against Alzheimer's disease. *Inflammopharmacology* **2020**, *28*, 95-110
75. Stansley, B.; Post, J.; Hensley, K. A comparative review of cell culture systems for the study of microglial biology in Alzheimer's disease. *J. Neuroinflammation* **2012**, *9*, 115-123
76. Franklin, A.; Stella, N. Arachidonylcyclopropylamide increases microglial cell migration through cannabinoid CB2 and abnormal-cannabidiol-sensitive receptors. *Eur. J. Pharmacol.* **2003**, *474*, 195-198
77. Han, Q. W.; Shao, Q. H.; Wang, X. T.; Ma, K. L.; Chen, N. H.; Yuan, Y. H. CB2 receptor activation inhibits the phagocytic function of microglia through activating ERK/AKT-Nurr1 signal pathways. *Acta Pharmacol. Sin.* **2022**, *43*, 2253-2266
78. Hauser, A. S.; Kooistra, A. J.; Munk, C.; Heydenreich, F. M.; Veprintsev, D. B.; Bouvier, M.; Babu, M. M.; Gloriam, D. E. GPCR activation mechanisms across classes and macro/microscales. *Nat. Struct. Mol. Biol.* **2021**, *28*, 879-888

79. Filipek, S. Molecular switches in GPCRs. *Curr. Opin. Struct. Biol.* **2019**, *55*, 114-120